Eye Diseases Monitoring using Ultrasound Technology

Safaa Makram Mohamed*, Ashraf Ali Wahba, Mohamed Ali Ahmed Eldosoky

Abstract— In this paper, new model implemented based on real images of disc topography and average retinal nerve fiber layer (RNFL) took from Topcon three dimensional optical coherence topography (Topcon 3D OCT) in ophthalmology institute of Cairo, Egypt, these images for different cases of normal, mild and severe glaucoma patients, in this model the ultrasound elastography technology applied on finite element model of human eye produced deformation according to different loads on optic disc region when stress 0.02 MPa applied on normal case, mild and severe glaucoma cases So the result average strain of normal patients= 0.379887, average strain of mild glaucoma patients = 0.510037 and average strain of severe glaucoma patients =1.079814 and compressed with stress 0.12 MPa applied on normal cases, mild and severe glaucoma cases So the result average strain of normal patients= 2.286461, average strain of mild glaucoma patients = 3.079613 and average strain of severe glaucoma patients =6.478117 to achieve early glaucoma detection and follow-up.

Index Terms— intraocular pressure; optic nerve head; retinal nerve fiber layer; disc topography, Topcon; glaucoma; ultrasound elastography; human eye model ; stress and strain analysis

1 INTRODUCTION

Glaucoma is the major ailment leading to blindness worldwide [1]. The increased of intraocular pressure (IOP) considered the critical reason for the progression of a disease. The mechanism by which increased IOP finally leads to destroy and loss of neural function is still indistinct [2-3]. Several recent publications have indicated that iop induced force and deformation (stress and strain) within optic disc region [2, 4-5]. Several analytical and computational models have been progressive for influence of optic nerve head (ONH) with geometry and mechanical properties of tissues [6-11].

There are factors used to reveal glaucoma as the RNFL thickness. Studies showed the perfect diagnostic parameter was inferior [12-13] of the average thickness of RNFL for glaucoma Other studies had the perfect diagnostic parameter was superior[14] of the average thickness of RNFL for glaucoma. The target of this paper was design finite element paradigm of human eye to detect IOP induced stress and strain analysis of optic disc region using ultrasound elastography technology

2 MATERIALS AND METHODS

2.1 Statuses of patients

The work was done on statuses of patients from the Institute of Ophthalmology of Cairo, Egypt and collected a medical reports that determine the type of case normal or glaucoma and during the preparation of the patient if the internal pressure of the patient eye is not measured, the doctor pressed the eyelid eye for diagnosis before using Topcon 3D OCT-2000 FA plus device. These measures have been made in a number of cases. The measurements on 4 Normal patients and 4 glaucoma patients in details 2 Normal cases, 2 Normal cases Caucasian, one mild glaucoma case, and 2 severe glaucoma cases. The device with high resolution technique to collect between OCT & fundus camera properties using IR images of disc topography and RNFL tomography, disc parameters are determined at the reference plane height of 120 µm from the Retina Pigment Epithelium (RPE) in this version, the instrument software then automatically calculated optic disc parameters arranged as normal, mild glaucoma and severe glaucoma as shown in Figure 1, 2.

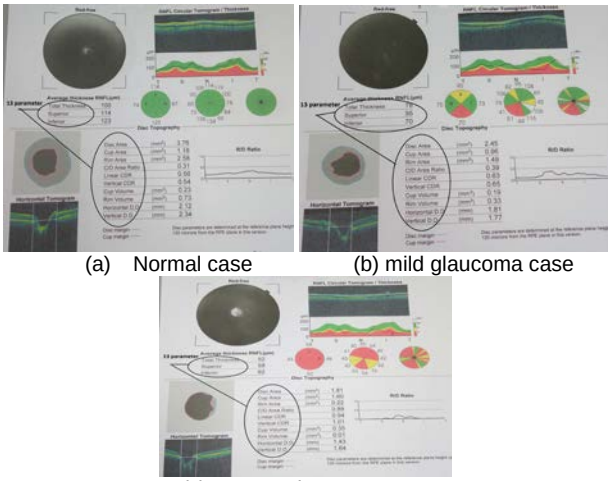

(a) Normal case (b) mild glaucoma case

(c) Severe glaucoma case

Fig. 1. Parameters for normal, mild and severe glaucoma case

- *Safaa Makram Mohamed is acorresponding author, faculty of engineering, biomedical engineering department, Helwan University, Cairo, Egypt, E-mail: eng.safaa78@gmail.com
- Ashraf Ali Wahba, faculty of engineering, biomedical engineering department, Helwan University, Cairo, Egypt, E-mail: ashraf_wahba@h-eng.helwan.edu.eg
- Mohamed Ali Ahmed Eldosoky, faculty of engineering, biomedical engineering department, Helwan University, Cairo, Egypt, E-mail: hm.eldosoky@gmail.com

2.2 Statistical analysis of data

Parameters took from Topcon device for each case were RNFL thickness parameters and disc topography parameters. Then, the values of average normal, mild and severe glaucoma patients of RNFL thickness parameters can be calculated in Table1 and Figure3 and the values of average normal, mild and severe glaucoma patients of disc topography parameters can be calculated in Table 2

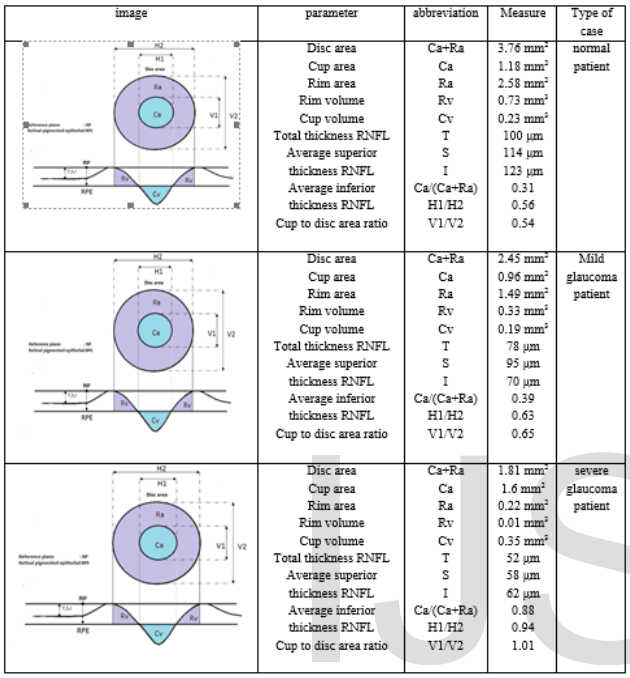

Fig. 2. Schematic of OCT parameters of disc topography at RPE of 120µm from reference plane of normal, mild glaucoma, severe glaucoma patient

TABLE 1
RNFL thickness of average normal, mild and severe Glaucoma cases

RNFL thickness parameters	unit	RNFL thickness of average normal cases	RNFL thickness of average mild glaucoma cases	RNFL thickness of average severe glaucoma cases
T	µm	74.25	73	46.33
S	µm	115.75	95	54.33
N	µm	96.75	75	50.67
I	µm	122	70	54
T	µm	74.25	73	46.33

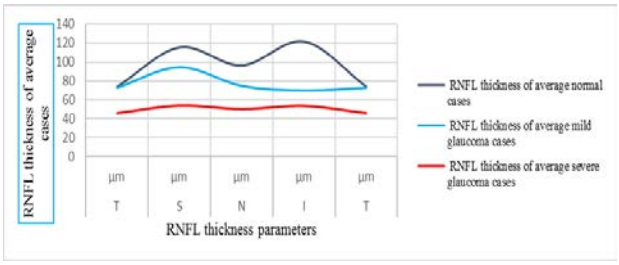

Fig. 3. RNFL thickness of average normal, mild and severe glaucoma cases

TABLE 2
Disc topography parameters of average normal, mild and severe glaucoma cases

disc topography parameters	unit	disc topography of average normal cases	disc topography of average mild glaucoma cases	disc topography of average severe glaucoma cases
Disc Area	mm2	3.3125	2.45	2.577
Cup Area	mm2	1.47	0.96	2.423
Rim Area	mm2	1.8425	1.49	0.16
C/D Area		0.4525	0.39	0.933
Linear CDR		0.6675	0.63	0.963
Vertical CDR		0.6625	0.65	1.003
CUP Volume	mm	0.5075	0.19	0.89
Rim Volume	mm	0.4175	0.33	0.01
Horizontal D.D	mm	2.0125	1.81	1.797
Vertical D.D	mm	2.095	1.77	1.797

2.3 Geometry of eye model

3-D model of the human eye is designed with the dimensions of actual human eye using ANSYS 17 software as shown in Table 3 [15] all data in table took from different sources [15-22]. The human eye is modeled with nine regions mentioned as cornea [16-17], aqueous humor[18] ,lens [17,19] , ciliary body ,iris [20] , vitreous humor [18] ,choroid , retina and sclera [21-22] as shown in Figure 4.

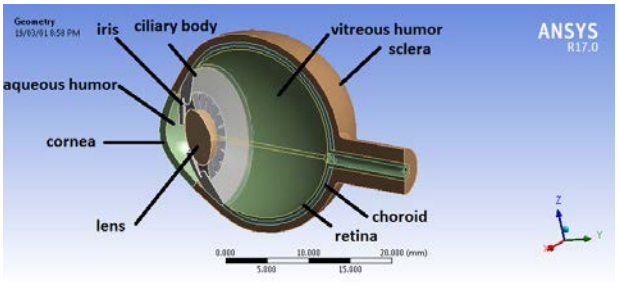

Fig. 4. Nine components of eye model

TABLE 3
Dimensions used to design model of eye

Component of eye	Dimension(mm)
Thickness of cornea	0.5
Outer radius of cornea	7.89
inner radius of cornea	6.7
Thickness of aqueous humor	3.05
Horizontal extension at lens of vitreous humor	16.4
Thickness of sclera	0.5
Radius of sclera	11.5
Diameter of pupil	3
Thickness of lens	4.2
Anterior radius of curvature of lens	11
posterior radius of curvature of lens	6

2.4 Material properties

Each region of the eye model is assumed to be homogeneous and isotropic [23]. Structural properties such as Young's modules of elasticity (E) [24-26], Poison's ratio (ϵ) [24-26] and density (ρ) [24, 27] for each component of eye model as shown in Table 4 all data in table took from different sources [23-27] .

2.5 Mesh

Tetrahedral free mesh of the model of eye is shown in Figure5, the details of elements and nodes for each case generated after meshing of geometry of eye model represented in Table 5

2.6 Load and boundary condition

Using ultrasound (US) probe as an imaging tool and a compression tool on the eye, respectively. Using the sclera which maintains the shape of the globe as fixed support

TABLE 4
Material properties of each component of eye

Component of eye	E(Mpa)	ϵ	ρ (Kg/m^3)
cornea	6.1	0.494	1400
Aqueous humor	0.037	0.49	999
iris	0.5	0.49	1100
Ciliary body	11	0.4	1600
lens	1.5	0.49	315
Vitreous humor	0.042	0.49	999
choroid	0.03	0.49	999
sclera	48	0.454	1400
retina	0.105	0.499	999

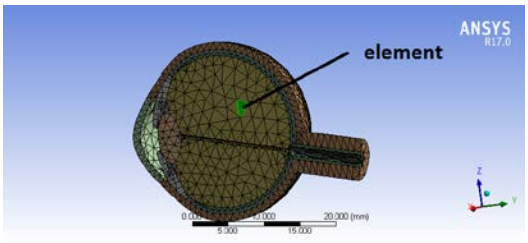

(a) elements of mesh

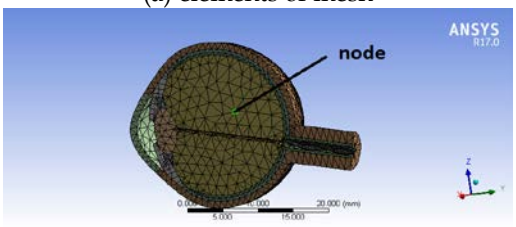

(b) nodes of mesh

Fig. 5. Tetrahedral free mesh of finite element eye model where: (a) element of mesh ,(b) node of mesh

TABLE 5
Elements and nodes for each case of eye model

cases	elements	nodes
Case1	28153	47796
Case 2	29412	49820
Case3	31229	51198
Case4	29790	50278
Case5	36029	58594
Case6	29639	47691
Case7	38060	63253
Case8	37796	60979

3 RESULTS

3.1 Result of statistical analysis of data

From Figure 3 the average thickness of RNFL smaller in average glaucoma cases than in average normal cases respectively in table 2 parameters such as disc area, rim area, rim volume smaller in glaucoma cases than in normal cases

3.2 Result of ANSYS

US probe compressed optic disc with stress 0.02 MPa applied on normal case, mild and severe glaucoma cases So the result average strain of normal patients= 0.379887, average strain of mild glaucoma patients = 0.510037 and average strain of severe glaucoma patients =1.079814 and compressed with stress 0.12 MPa applied on normal cases, mild and severe glaucoma cases So the result average strain of normal patients= 2.286461, average strain of mild glaucoma patients = 3.079613 and average strain of severe glaucoma patients =6.478117 in Figure 6

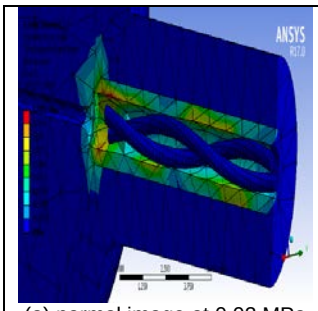
(a) normal image at 0.02 MPa

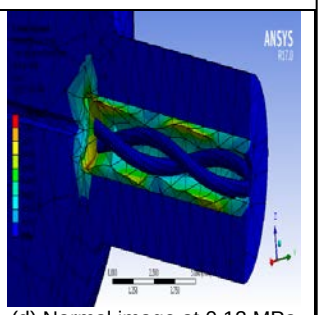
(d) Normal image at 0.12 MPa

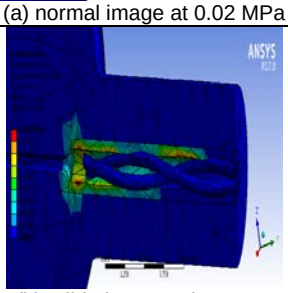
(b) mild glaucoma image at 0.02 MPa

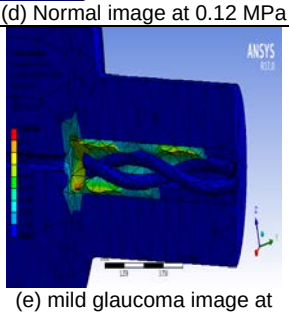
(e) mild glaucoma image at 0.12 MPa

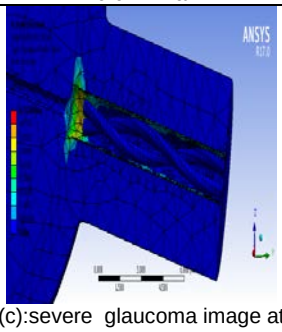
(c):severe glaucoma image at 0.02 Mpa

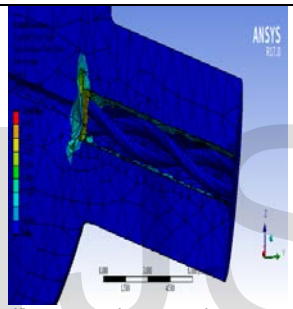
(f) severe glaucoma image at 0.12 MPa

Fig. 6. Normal, mild and glaucoma image at 0.02 MPa and 0.12 MPa

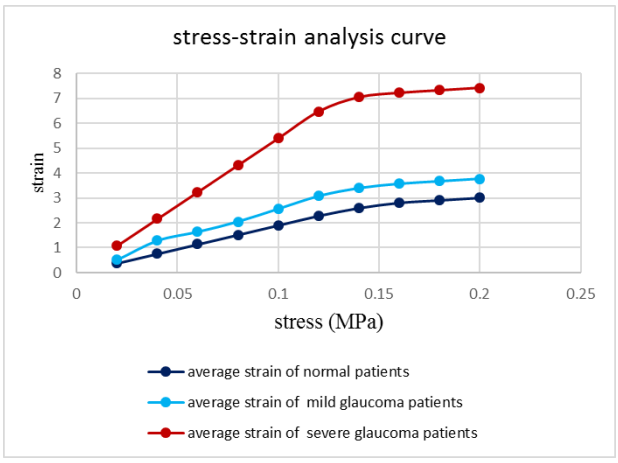

Fig. 7. Stress-strain analysis curve of normal, mild and severe glaucoma patients

3.3 stress-strain analysis

when load is applied using US probe acted as stress on the proposed portion this occur when optic disc region compressed with different stresses from 0.02MPa to 0.2MPa, the effect caused strain small in average normal cases and large in average glaucoma cases from stress-strain analysis the average data of normal, mild and severe glaucoma patients differentiated (see Figure 7 and Table6)

Table 6
Stress-strain analysis of normal, mild and severe glaucoma patients

stress (MPa)	average strain of normal patients	average strain of mild glaucoma patients	average strain of severe glaucoma patients
0.02	0.379887	0.510037	1.079814
0.04	0.761149	1.285266	2.159583
0.06	1.142457	1.640257	3.239303
0.08	1.523784	2.05304	4.318969
0.1	1.905122	2.567318	5.398575
0.12	2.286461	3.079613	6.478117
0.14	2.6	3.4	7.05
0.16	2.8125	3.575	7.225
0.18	2.9125	3.675	7.325
0.2	3.0125	3.775	7.425

4 Conclusion and Discussion

Finite element modeling of human eye showed that normal patient can be calculated according to the relation

$$y = 1.2604\ln(x) + 4.9607$$

Where y represented strain obtained from normal cases and x represented stress applied on normal cases respectively,

$$y = 1.5299\ln(x) + 6.2302$$

Where y represented strain obtained from mild glaucoma cases and x represented stress applied on mild glaucoma cases Respectively,

$$y = 3.1399\ln(x) + 12.711$$

Where y represented strain obtained from severe glaucoma cases and x represented stress applied on severe glaucoma cases to achieve early glaucoma detection and follow-up.

References

[1] H. Quigley, "and 2020," pp. 262–267, 2020.

[2] C. F. Burgoyne, J. C. Downs, A. J. Bellezza, J.-K. F. Suh, and R. T. Hart, "The optic nerve head as a biomechanical structure: a new paradigm for understanding the role of IOP-related stress and strain in the pathophysiology of glaucomatous optic nerve head damage," Prog. Retin. Eye Res., vol. 24, no. 1, pp. 39–73, 2005.

[3] H. C. Geijssen, Studies on normal pressure glaucoma. Kugler Publications, 1991.
[4] I. A. Sigal, "Interactions between Geometry and Mechanical Properties on the Optic Nerve Head," vol. 50, no. 6, 2018.
[5] I. A. Sigal, J. G. Flanagan, I. Tertinegg, and C. R. Ethier, "Predicted extension, compression and shearing of optic nerve head tissues," Exp. Eye Res., vol. 85, no. 3, pp. 312–322, 2007.
[6] E. A. Sander, J. C. Downs, R. T. Hart, C. F. Burgoyne, and E. A. Nauman, "A cellular solid model of the lamina cribrosa: mechanical dependence on morphology," J. Biomech. Eng., vol. 128, no. 6, pp. 879–889, 2006.
[7] I. A. Sigal, J. G. Flanagan, I. Tertinegg, and C. R. Ethier, "Reconstruction of human optic nerve heads for finite element modeling," vol. 13, pp. 313–329, 2005.
[8] H. Dongqi and R. Zeqin, "A biomathematical model for pressure-dependent lamina cribrosa behavior," J. Biomech., vol. 32, no. 6, pp. 579–584, 1999.
[9] M. E. Edwards and T. A. Good, "Use of a mathematical model to estimate stress and strain during elevated pressure induced lamina cribrosa deformation," Curr. Eye Res., vol. 23, no. 3, pp. 215–225, 2001.
[10] A. J. Bellezza, "Biomechanical properties of the normal and early glaucomatous optic nerve head: An experimental and computational study using the monkey model.," 2003.
[11] I. A. Sigal, J. G. Flanagan, I. Tertinegg, and C. R. Ethier, "Modeling individual-specific human optic nerve head biomechanics. Part I: IOP-induced deformations and influence of geometry," Biomech. Model. Mechanobiol., vol. 8, no. 2, pp. 85–98, 2009.
[12] C. K. S. Leung et al., "Comparison of macular and peripapillary measurements for the detection of glaucoma: an optical coherence tomography study," Ophthalmology, vol. 112, no. 3, pp. 391–400, 2005.
[13] M.-L. Huang and H.-Y. Chen, "Development and comparison of automated classifiers for glaucoma diagnosis using Stratus optical coherence tomography," Invest. Ophthalmol. Vis. Sci., vol. 46, no. 11, pp. 4121–4129, 2005.
[14] K. Nouri-Mahdavi, D. Hoffman, D. P. Tannenbaum, S. K. Law, and J. Caprioli, "Identifying early glaucoma with optical coherence tomography," Am. J. Ophthalmol., vol. 137, no. 2, pp. 228–235, 2004.
[15] S. Das and M. S. M, "FEM MODELLING OF HUMAN EYE FOR INVESTIGATING THE THERMAL EFFECTS OF TUMOR ON THE OCULAR SURFACE TEMPERATURE," vol. 12, no. 23, pp. 6741–6754, 2017.
[16] P. A. Tsonis, Animal models in eye research. Academic Press, 2011.
[17] C. N. Wilson, "A Fully Customizable Anatomically Correct Model of the Crystalline Lens." Université d'Ottawa/University of Ottawa, 2011.
[18] N. Heussner et al., "Thermodynamic Finite-Element-Method (FEM) eye model for laser safety considerations," in Optical Interactions with Tissue and Cells XXIV, 2013, vol. 8579, p. 85790J.
[19] D. Malacara-Hernández and Z. Malacara-Hernández, Handbook of optical design. CRC Press, 2016.
[20] S. Thainimit, L. A. Alexandre, and V. M. N. De Almeida, "Iris surface deformation and normalization," in Communications and Information Technologies (ISCIT), 2013 13th International Symposium on, 2013, pp. 501–506.
[21] R. E. Norman et al., "Dimensions of the human sclera: thickness measurement and regional changes with axial length," Exp. Eye Res., vol. 90, no. 2, pp. 277–284, 2010.
[22] P. G. Watson, B. L. Hazleman, and C. E. Pavesio, The sclera and systemic disorders. JP Medical Ltd, 2012.
[23] V. Shukla, "FEA Investigation of a Human Eye Model Subjected To Intra-Ocular Pressure (IOP) and External Pressure," no. March, 2017.
[24] J. Al-sukhun, C. Lindqvist, and R. Kontio, "Modelling of orbital deformation using finite-element analysis," no. May 2014, 2006.
[25] C. Clemente, L. Esposito, N. Bonora, J. Limido, J. L. Lacome, and T. Rossi, "Traumatic eye injuries as a result of blunt impact: computational issues," in Journal of Physics: Conference Series, 2014, vol. 500, no. 10, p. 102003.
[26] A. S. Roy and W. J. Dupps, "Effects of altered corneal stiffness on native and postoperative LASIK corneal biomechanical behavior: a whole-eye finite element analysis," J. Refract. Surg., vol. 25, no. 10, pp. 875–887, 2009.
[27] U. Cicekli, "Computational model for heat transfer in the human eye using the finite element method," 2003.